# Oxidation and creep properties at 1200 °C of cast quaternary Ni-Cr-C-Ti alloys

Patrice Berthod, Estelle Kretz, Floriane Allègre, Mélissa Ritouet, Thierry Schweitzer, Lionel Aranda

# Oxidation and creep properties at 1200°C of cast quaternary Ni-Cr-C-Ti alloys

**Patrice Berthod*, Estelle Kretz, Floriane Allègre, Mélissa Ritouet, Thierry Schweitzer, Lionel Aranda**

Institut Jean Lamour, Department N°2: Chemistry and Physic of Solids and Surfaces
Team “Surface and interface, chemical reactivity of materials”
Faculty of Sciences and Techniques, Nancy – University,
B.P. 70239, 54506 Vandœuvre-lès-Nancy – France

*Corresponding author, email: pberthodcentralelille1987@orange.fr

*Post-print of the article* **Materials Science & Engineering A 699 (2017) 145–155.**
http://dx.doi.org/10.1016/j.msea.2017.05.089

**Abstract:** Three nickel-based alloys rich in chromium (25wt.%) and containing carbon and titanium in quantities chosen to promote the appearance of titanium carbides (0.25C-1Ti, 0.50C-1Ti and 0.50C-2Ti, in wt.%) were elaborated by casting in inert atmosphere. Their microstructures and their thermodynamic, chemical and mechanical behaviours at high temperature were studied. The as-cast microstructures of the obtained alloys are composed of a dendritic nickel matrix and of interdendritic carbides. These carbides are not TiC as expected, but $Cr_7C_3$, the whole titanium remaining in solid solution in the matrix. The applied {46h, 1200°C}-exposure in air led to the development of an external duplex oxide scale constituted of a thick inner chromia scale and a thin outer rutile scale. These oxide layers resisted spallation more than the ones of Ti-free ternary reference alloys in similar conditions. The bulk’s chromium carbides became rounder and coarsened, with as result a decrease in room temperature hardness. The {5 or 20 MPa, 1200°C}-3 points flexural creep tests showed a rather good behaviour, regarding the high test temperature. It is concluded that titanium seems hardening these bases of alloys at low and high temperatures. However the effects on the oxidation behaviour may be deleterious for the oxidation rate and subsurface Cr-impoverishment. In contrast Ti appears as beneficial for the resistances against spallation and possibly chromia volatilization. This needs to be further investigated.

**Keywords:** electron microscopy (A); mechanical characterization (A); nickel based superalloys (B); casting (C); aging (D); oxidation (D);

## 1. Introduction

The constant increase in energy efficiency of aero-engines and power generation turbines leads to higher and higher working temperatures. The resulting need of metallic materials for the hottest components induces the development of more and more sophisticated superalloys. By comparison with the ones existing several decades ago [1, 2], chemical compositions and microstructures respectively contain more elements and more strengthening phases [3]. Titanium is on the one hand the base of various alloys for biomedical [4] or structural aeronautical parts [5]. On the other hand one it also features among the key alloying elements, by playing a particularly important role in numerous superalloys [6-8] and $Ti_3Al$ or TiAl aluminides [9-11]. Titanium may notably be present in the γ' intermetallic compound [12-14] or η phase [15] with often high benefit for the mechanical properties of the alloys at high temperature [16]. The effects of the present titanium on the high temperature behaviour of the superalloys is not limited to the mechanical field but this highly oxidable element [17, 18] may be also involved in the oxidation progress by leading to $TiO_2$ rutile oxides [19, 20].

More known as a base element for low density structural alloy or as a γ'-former element, it can be underlined that titanium is also a rather {strong MC carbide}-former metal, allowing the presence of TiC carbides such as in simple cast chromium-rich cobalt-based alloys as recently shown [21]. In these cobalt-chromium alloys titanium led, in presence of carbon of about the same atomic content as Ti, to the development of eutectic TiC carbides whose script-like morphology is known to be favourable to mechanical resistance at high temperature. It can be thus interesting to observe the microstructures which may result from the addition of Ti and C in cast nickel-chromium (25wt.%) alloys. Such alloys are already known to be intrinsically resistant against oxidation by hot gases and corrosion by molten substances thanks to high content in chromium and to a nickel matrix through which Cr atoms can rather easily diffuse. Characterizing the high temperature oxidation and creep behaviours can be therefore interesting to do on such (Ti, C)-added versions.

## 2. Experimental details

### 2.1 Elaboration of the alloys

Three alloys were here considered. They are similar to the Co(bal.)-25Cr-xC-yTi cast alloys recently studied [21], thus with (x,y) = (0.25, 1), (0.50, 1) and (0.50, 2). But they are here based on nickel instead cobalt. These three alloys were elaborated following the same procedure as the Co-based alloys recently studied:

- Charge to melt: pure parts of Ni, Cr, C et Ti (Alfa Aesar, purity > 99.9wt.%)
- Furnace: high frequency induction technology, 50kW max (CELES, France), 110kHz-5kV max. during melting
- Atmosphere: 300 mbars of pure argon
- Thermal cycle: heating taking about 2 minutes until obtaining the liquid state of the alloy, dwell for 3 minutes at maximal voltage to allow total chemical homogenization of the molten alloy
- Rather rapid decrease in power to achieve the liquid state cooling (about 10 seconds), the alloy solidification (about 25 seconds) and the solid state cooling in contact with a water-cooled copper crucible (about 15 minutes).

Two ternary alloys with the same Ni, Cr and C contents earlier prepared following the same procedure and studied in oxidation by air according to the same parameters as here [22], were also considered. They allowed having Ti-free versions of these first three alloys for observing the impact of the presence of Ti on the obtained microstructures and the high temperature oxidation behaviours of the alloys.

### 2.2 Metallographic preparation and observations

The obtained ingots were thereafter cut, first using a Buehler Abrasimet Delta to get separated raw parts, and second a Buehler IsoMet 5000 linear precision saw to prepare more accurately the samples for the thermal analyses, the oxidation exposures and the creep tests. One of the raw parts, per alloy, was embedded in a cold resin mixture (CY230 + hardener HY956 from ESCIL, France). Grinding with SiC papers with roughness range extended from 24 to 1200-grit, followed by ultrasonic cleaning and polishing with textile enriched in 1µm hard particles, led to mirror like states allowing microstructure characterization.

This was done using a tungsten filament Scanning Electron Microscope (SEM) of the JSM6010LA type (JEOL, Japan), together with its attached Energy Dispersion Spectroscopy device. The microstructure observations were essentially done under 20kV in the Back Scattered Electrons mode (BSE) at magnifications ranging from ×120 to ×1000. The EDS measurements were carried out in full frame mode (global chemical composition) and in spot mode (compositions of the different phases).

### 2.3 Fusion and solidification temperature ranges

Preliminarily to the high temperature tests, the melting ranges of the three alloys were measured. First samples with approximate dimensions 2 mm × 2 mm × 8 mm were machined using the IsoMet5000 precision saw, and second they were placed in an alumina crucible inside a TG-ATD 92.16-18 (SETARAM, France) thermogravimetry & differential thermal analysis apparatus. A two phase heating was applied at +20 K $min^{-1}$ until 1200°C then at +5 K $min^{-1}$ until 1500°C, followed by a two phase cooling achieved at -5 K $min^{-1}$ until 1200°C then at -20 K $min^{-1}$ until room temperature. The obtained heat flow curves were thereafter exploited to know the temperatures of fusion start and end, and of solidification start and end. The resulting approached value of solidus temperature was then considered to be sure that the following tests can be really done (alloys still wholly solid).

### 2.4 Bulk and surface stability at high temperature

In other raw parts of each ingot parallelepipeds, compact for the exposures at high temperature and elongated for the creep tests (next paragraph) were machined using the IsoMet 5000 precision saw. The dimensions of the samples devoted to the exposures at high temperature were approximately 10 mm × 10 mm × 3 mm. They were ground on their six main faces and rounded on their edges and corners using 1200-grit SiC papers. These samples were placed in a tubular resistive furnace in which they were exposed to air at 1200°C during 46 hours, after a heating done at +20 K $min^{-1}$ and before a cooling done at -5 K $min^{-1}$. This rather low cooling rate was chosen to minimize the loss in external oxide scale.

After return to room temperature the samples were carefully extracted out of the furnace and their oxidized surfaces were photographed and submitted to X-ray

diffraction (Philips X'Pert Pro, Cu Kα, λ = 1.5406 Å). There were gold-coated by cathodic pulverisation, nickel-coated by electrolytic deposition in a 50°C-heated Watt's bath under 1.6 A/dm² during 2 to 3 hours, then cut in two parts using the IsoMet 5000 precision saw. The prior Ni coating allowed keeping the major part of the external oxide scales.

After the same metallographic preparation as previously described in the 2.2 paragraph, the obtained cross sections were characterized using the same SEM equipped with its EDS apparatus. The external and internal oxides were observed in BSE mode while EDS spot analysis was carried out to specify the observed oxides and to value the chemical composition in the alloy very close to the interface with the oxides scales. EDS was also used for obtaining the concentration profiles from this interface towards the first zone of the bulk not affected by oxidation.

The microstructures in the bulk were also examined in order to evaluate the eventual microstructure changes induced by the high temperature exposure. Hardness tests were carried out according to the Vickers method, using a Testwell Wolpert machine. Five indentations under a 10kg load led to an average value and a standard deviation value for the three alloys, in their aged state as well as in their as-cast condition.

### 2.5 Three-points flexural creep tests

All the three alloys were submitted to centred three-points flexural creep tests, using a TMA 92.16-18 thermodilatometer (SETARAM, France) equipped with a device allowing performing this type of mechanical test at high temperature.

Accurate cutting and polishing until mirror state allowed obtaining parallelepipeds with the following dimensions:

- Length: 15 mm
- Width: 2 mm
- Thickness: 1 mm

The total length was in all cases 2 to 3 mm greater than the space between the two bottom alumina supports. The width and thickness samples were accurately controlled to be sure that they varied less than 0.01mm all along each sample. Their exact values were taken into account to choose the load to apply with the upper central alumina support in order to obtained exactly 20 MPa in the central bottom surface of the sample. This load was carefully progressively applied at room temperature, and maintained constant during all the heating (at +20K $min^{-1}$), the isothermal stage at 1200°C (100 hours, or less if too rapid deformation and contact with the bottom alumina base, after a 1.4 mm deformation) and the cooling (-20K $min^{-1}$). The displacement of the centre of the sample was recorded using the sensor of the dilatometer. Additional tests were also carried out, at the same temperature but by applying a lower load calculated to induce 5 MPa in the central bottom surface of the sample. The principle of the test is illustrated by a scheme given in Figure 1.

## 3. Results

### 3.1 As-cast microstructures of the obtained alloys

General views of the microstructures of the three alloys in their as-cast states are provided in Figure 2. They are all double-phased with a dendritic matrix and dark

carbides disposed in the interdendritic spaces. The interdendritic carbide network is logically denser for a higher carbon content.

More detailed view can be examined in Figure 3. These carbides, of the $Cr_7C_3$ nature as first suggested by their acicular shape and second confirmed by spot EDS analysis, obviously form a eutectic compound with the matrix. Few black particles are also present. They are too fine to be analysed but spot EDS analyses showed high concentrations in O and/or N, sometimes together with C.

Global EDS analyses confirm that the targeted contents in Cr and Ti were well obtained:

- 25.4 ±0.1wt.% Cr and 1.0 ±0.1wt.% Ti for the Ni-25Cr-0.25C-1Ti alloy,
- 25.7 ±0.1wt.% Cr and 1.1 ±0.1wt.% Ti for the Ni-25Cr-0.50C-1Ti alloy
- 25.5 ±0.3wt.% Cr and 2.1 ±0.1wt.% Ti for the Ni-25Cr-0.50C-2Ti alloy

It was not possible to verify the content in carbon because of both its too low molar weight and its low expected contents. However we can consider that it is itself well respected since first the used elaboration procedure never led to any loss in carbon and second that the carbide quantities are typical of these 0.25 and 0.50wt.% contents in C, compared to many earlier studied alloys based on Ni, Co or Fe with 25 to 30wt.%Cr (C contents verified by spark spectrometry for some of them).

### 3.2 Fusion's start temperatures

Differential thermal analysis was carried out for each of these three alloys. The DTA curves (example in Figure 4), show that, during heating, the three alloys started melting at temperatures close to 1300°C (the three values are between 1296°C and 1312°C) and finished solidifying close to 1250°C (values between 1248 and 1326°C). All these temperatures are higher than 1200°C, temperature chosen for the isothermal exposures and the creep tests. In all cases, melting finished and solidification started at temperatures equal to or lower than 1400°C.

These preliminary thermal analysis tests thus showed the possibility to perform the following oxidation and creep test at 1200°C, without risking local start of fusion.

### 3.3 Exposures at 1200°C: surface states

The exposures of the three alloys during 46 hours at 1200°C in air led to the deterioration of their surfaces with notably the formation of external oxide scales. Almost no oxide spallation during the slow cooling occurred and the main part of these oxide scales remained on surface, in contrast with what earlier took place for the Ti-free alloys (Figure 5).

Before cutting them for the cross-section preparation, the three oxidized samples were subjected to X-ray diffraction. As shown on the obtained diffractograms (example of Ni-25Cr-0.50C-1Ti in Figure 6) it seems that two oxides are particularly present:

- chromia, in which titanium is seemingly present in low quantity (the correspondence is the best with $(Cr0.88Ti0.12)_2O_3$
- and titanium oxide $TiO_2$ (rutile).

Some other peaks may correspond to titanium nitrides (TiN0.90) and carbo-nitrides (TiC0.51N0.12).

Observed in cross-section (Figure 7 for the Ni-25Cr-0.25C-1Ti alloy, Figure 8 for the Ni-25Cr-0.50C-1Ti one and Figure 9 for the Ni-25Cr-0.50C-2Ti one) one can see first that the external oxide scale is composed of two successive layers. The outer one, probably partly removed by a little spallation during cooling and/or by machining during the cross-sections preparation, is made of $TiO_2$ (average thickness of 2 µm for the two 1wt.%Ti-containing alloys and of 4 µm for the 2wt.%Ti-containing one). The second one, rather porous, is made of a Ti-containing chromia: atomic contents in Cr and O very close to the 3/2 ratio but with presence, in this chromia scale, of 0.35 to 0.45 at.% Ti (0.5-0.7 wt.%Ti) in the two 1wt.%Ti-containing alloys and of 0.65-0.70 at.%Ti (0.9-1.1 wt.%Ti) for the 2wt.%Ti-containing one. The average thicknesses of this internal chromia scale are around 30 µm for the three alloys. This is significantly higher than the average of 20 µm of chromia earlier observed on the surface of the Ti-free corresponding alloys after oxidation in the same condition (Figure 10). Additionally the chromia scales formed on these two ternary alloys were not so porous. Another difference between the Ti-containing alloys studied here and the Ti-free ones earlier studied is, for the former ones, the presence of internal oxides in the subsurface close to the interface. The ternary alloys were not affected by internal oxidation.

### 3.5 Exposures at 1200°C: subsurface states

The subsurface states are first characterized by the loss of carbides over a depth which varies with the considered alloy. Furthermore these carbide-free zones more or less correspond to the chromium-depletion depths (illustrated by the concentration profiles given in Figure 11 for the Ti-free alloys and in Figure 12 for the two reference Ti-free alloys). Indeed the carbide-free depths are of about 160 µm (Cr-depleted depth: about 160 µm) for the Ni-25Cr-0.25C-1Ti alloy, of about 130 µm (Cr-depleted depth: about 135 µm) for the Ni-25Cr-0.50C-1Ti alloy, and of about 120 µm (Cr-depleted depth: about 125 µm) for the Ni-25Cr-0.50C-2Ti alloy. Thus the carbide-free depths and the chromium-depleted depths are significantly lower in the case of the carbon contents, and then the carbide fractions, are higher.

These carbide-free depths are similar to the ones earlier observed for the two ternary alloys oxidized in the same conditions (about 170 µm and 120 µm for the Ni-25Cr-0.25C and Ni-25Cr-0.50C alloys respectively; here too similar to their chromium-depleted depths). The main difference between the Ti-containing alloys and the Ti-free ones is the Cr concentration gradient: approximately 0.09 wt.%Cr / µm for the Ni-25Cr-0.25C-1Ti alloy against 0.02 wt.%Cr / µm for the Ni-25Cr-0.25C reference alloy, and 0.07-0.08 wt.%Cr / µm for the Ni-25Cr-0.50C-1Ti and Ni-25Cr-0.50C-2Ti alloys against 0.025 wt.%Cr / µm for the Ni-25Cr-0.50C reference alloy. The chromium contents in extreme surface are between 10 and 12 wt.%Cr for the three Ti-containing alloys against between 18 and 20 wt.%Cr for the two reference ternary alloys.

The three Ti-containing alloys also present a zone depleted in titanium, which extends from the scale/alloy interface (Ti content almost equal to zero) to the bulk, over a much higher depth than the Cr-depleted one. The Ti gradient, almost linear, continues in the still carbides-containing zone.

### 3.6 Exposures at 1200°C: bulk states and hardness evolution

In the centre of each aged sample it was possible to observe how the 46 hours spent at 1200°C modified the microstructures. As illustrated by some SEM/BSE micrographs in Figure 13 for the three Ti-containing alloys and in Figure 14 for the two Ti-free reference alloys, the acicular shape of the carbides was lost during the high temperature exposure. These ones became much rounder. No evident difference of behaviour in this field can be noticed for the Ti-containing alloys by comparison with the Ti-free ones. The carbides are still $Cr_7C_3$ carbides in all cases.

These changes in the carbides' morphologies induced a significant decrease in room temperature hardness for all alloys (Figure 15). In their as-cast states the Ti-containing alloys tended to be slightly harder than the Ti-free ones for a given carbon content. After aging the decrease in hardness was lower for the Ti-containing alloys than for the Ti-free ones, allowing the former to present hardness values significantly higher than the latter ones. However, whatever the state (as-cast or aged) the three 0.50C-containing alloys remain harder than the two 0.25C-containing ones.

### 3.7 Flexural creep tests at 1200°C under 20 MPa or 5 MPa

When the applied load induced a 20MPa constant tensile stress in the middle of the bottom of the sample, the deformation of the three alloys was initially particularly fast: linear at a constant speed of about 0.3 mm $s^{-1}$ (i.e. nearly 80 µm $h^{-1}$). After around 7h deformation started decreasing to seemingly stabilize at a new constant deformation rate between 10 and 20 µm $h^{-1}$, this depending on the alloy (Figure 17). This new deformation regime looks like secondary creep. The steady state deformation rate is of approximately 12 µm $h^{-1}$, 9 µm $h^{-1}$ and 18 µm $h^{-1}$ for the Ni-25Cr-0.25C-1Ti, Ni-25Cr-0.50C-1Ti and Ni-25Cr-0.50C-2Ti alloys, respectively. Deformation went on during about ten hours before contact of the lowest part of the sample with the base of the apparatus (start of the horizontal end of the deformation curves).

For a resulting 5 MPa induced tensile stress, it seems that the primary stage of creep is much shorter for the Ni-25Cr-0.25C-1Ti and Ni-25Cr-0.50C-2Ti alloys, in term of both time and corresponding deformation (Figure 18). In fact, thereafter, deformation goes on decelerating and stabilization in secondary creep is not really reached after 50 hours of test. In the case of the Ni-25Cr-0.50C-1Ti alloy secondary creep starts after about 10 hours and a really linear deformation can be observed. The deformation rates recorded after fifty hours of test are all between 1 and 4 µm $h^{-1}$, which is remarkably low regarding the temperature level.

## 4. Discussion

One already knew to which type of microstructures casting of quaternary nickel-based (and also cobalt-based and iron-based) alloys containing 25 to 30 wt.%Cr, 0.2 to 0.5wt.%C and moderate contents in MC-former elements may usually lead. This is thus unsurprisingly that the three alloys studied here are composed of a dendritic matrix and of interdendritic carbides mixed with matrix in a double-phased compound obviously of a eutectic nature. Contrariwise the kind of the obtained carbides was not expected since the MC-type carbides generally tend to be more stable than chromium carbides at high temperature. Indeed the formation enthalpies

($\Delta G_f°(T)$) related to one mole of carbon are, for 1200°C (1473K), -31kcal/mol for NbC, -34kcal/mol for TaC, -40kcal/mol for TiC or -41kcal/mol for ZrC … against -17kcal/mol for chromium carbides [23]. However the coexistence with the other phases in the alloy (notably the matrix) is of course to be taken into account and results can be different from what can occur in cobalt-based and iron-based alloys [21,24, 25]. In the specific case of titanium, it was observed here that the most stable state for a {titanium and carbon}-containing nickel alloy so rich in chromium is the mixture of a nickel solid solution containing all the Ti atoms and of chromium carbides, and not the mixture of a nickel solid solution containing all the Cr atoms and of titanium carbides. In such chromium-rich nickel-based alloys, this is thus different from HfC [22] or NbC [26], but similar to TaC [27].

The $Cr_7C_3$ carbides appeared instead the TiC ones are also accompanied by some very stable small particles of titanium oxides or nitrides which logically remain in the microstructure after high temperature aging, unlike the few TiC particles which appeared besides the numerous chromium carbides during the fast solidification. This limited oxidation or nitridation of a part of titanium took place during the elaboration despite the inert atmosphere (pure argon with only few ppm of $O_2$ and $N_2$). It seems to be not avoidable and one can unfortunately think that they can play a detrimental role on the high temperature mechanical properties.

The exposure in air at 1200°C for a rather long time led to oxidation of the samples' surfaces. Selective oxidation occurred twice: oxidation of chromium and oxidation of titanium. As usually observed for {chromium carbides}-containing chromia-forming alloys, an external continuous chromia scale developed on the sample surface. At the same time a chromium-depleted zone developed in the subsurface towards the sample centre. Similar phenomena also occurred for titanium: an external continuous $TiO_2$ scale and a Ti-depleted zone in subsurface towards the sample centre, too. During the -5K $min^{-1}$ cooling this duplex external oxide scales resisted oxide spallation better than the Ti-free reference ternary alloys the single external chromia scale of which was partly lost. One can wonder whether the thin outer $TiO_2$ scale allowed the thicker internal chromia scale staying on the alloys, or whether the small internal $TiO_2$ oxides observed in the subsurface close to the oxide/metal interface plaid a scale-pegging role. Since some titanium seemed existing in the chromia scale (revealed by both XRD and EDS), the presence of this element perhaps modified a little the behaviour of chromia during the cooling. It also true that this Ti—containing chromia scale seemed more porous than the chromia scales formed over the two Ti-free reference ternary alloys. This difference may be first pointed out concerning the faster oxidation of the Ti-containing alloys (thicker chromia scale, more severe chromium-impoverishment of the subsurface) than for the reference alloys. It allowed maybe also the chromia scale better accommodate the compressive stresses developed during cooling due to the mismatch in thermal expansion or retraction behaviour between oxide scale and alloy.

As usually observed for carbides containing alloys, a carbide-free zone developed towards the sample's centre in all cases. Here too the carbide-free depth well corresponds to the zone depleted in the carbide-former element (here Cr for both the Ti-containing and Ti-free alloys since titanium did not led to carbides), as systematically observed for Cr in chromia-forming {chromium carbides}-containing alloys and for Ta in (external chromia+ internal $CrTaO_4$)-forming TaC-containing alloys. The Ti-depletion in matrix is more extended than the one in Cr. The reason is that the dissolving chromium carbides feeds the neighbour matrix in Cr, this

explaining the correspondence of the carbide-free zone and of the Cr-depleted zone, while no such feeding in Ti from carbides is possible of course.

Concerning the depths of the carbide-free zones, these ones are, as usual, lower for the alloys with high carbon content than for the ones with low carbon content. But, for a given carbon content, no difference in carbide-free depth exists between the Ti-free and the Ti-containing alloys. Titanium has obviously not any influence on that. In contrast, the presence of Ti in solid solution in the carbide-free zone and deeper, even if its content is lower than as in the bulk, seems partly obstructing the diffusion of Cr towards the oxidation front, as suggested by the higher Cr-concentration gradients in the subsurface for the Ti-containing alloys than for the Ti-free ones. This is another deleterious effect of Ti on the oxidation behaviour, to be added to the porous chromia scale. Because of that, the Cr content in extreme surface (close to the oxidation front) is particularly low for the Ti-containing alloys by comparison with the reference ternary alloys, which may threaten the chromia-forming behaviour of these Ti-containing alloys.

The 1200°C stages induced significant evolution in morphology for the acicular eutectic chromium carbides. These ones became coarsened and rounder, with the loss of their efficiency in imbrication of neighbour matrix dendrites. This concerns the Ti-containing alloys as well as the Ti-free reference ones. A long morphologic stability of a script-like eutectic carbides interdendritic network was what was expected by adding Ti, element known as a strong MC-former one. The lack in stability of TiC carbides in such nickel-chromium alloys, by comparison to chromium carbides did not permit to benefit of this efficient strengthening effect that MC carbides may bring to cast alloys. However, the resistance against creep of the studied Ti-containing nickel-based alloys was rather good by taking in consideration the high level of the test temperature (1200°C). This is already true for an induced tensile stress equal to 20 MPa, for which the deformation curve starts with a long primary creep but continues with a slow secondary one (unfortunately not observable on long times due to the contact between sample and the apparatus base). The resistance of these alloys against creep becomes particularly interesting for 5 MPa, with a much lower deformation rate in secondary stage. One can think that this unexpected good creep-resistance (for alloys containing only chromium carbides) can be attributed to the presence of Ti atoms in solid solution in the matrix, together to the presence of interdendritic carbides. It is true that, already at room temperature, the hardness of the Ti-containing alloys were higher than the ones of the Ti-free reference alloys. Since a few TiC carbides were present beside the numerous chromium carbides in the as-cast alloys and disappeared during the 1200°C, with as result an increase in content of Ti atoms in solid solution, it was possible to value the distortion induced by Ti in the face centred cubic crystalline network of the matrix, by XRD experiments on a same alloy in the two states (as-cast and aged at 1200°C). This was done and the obtained diffractograms (case of Ni-25Cr0.5C-2Ti displayed in Figure 19) reveal a slight shift of the matrix peaks toward higher angles. According to the Bragg's law this suggests a decrease in cell parameters, which results from the smaller size of the Ti atoms in comparison with nickel and chromium. One can thus effectively envisage a stress field at the atomic scale, and therefore a strengthening effect of the presence of Ti in solid solution.

## 5. Conclusions

Thus, adding Ti for form MC-carbides in nickel alloys was obviously not as successful as the addition of Hf or Nb in similar alloys or the additions of Ti in cobalt-chromium and iron-chromium alloys. The carbides nature, morphology and repartition were almost not modified by the introduction of this fourth element in the Ni-Cr-C ternary bases taken here as reference alloys. However the presence of Ti in solid solution probably hardened the matrix with as results a higher hardness at room temperature. This also explains the rather good creep resistance by comparison to what can be expected for alloys of simple composition, elaborated by conventional casting, based on nickel (and not on cobalt) and containing only chromium carbides. Beside this rather good effect on the mechanical properties (obviously achieved by solid solution strengthening instead the expected but not obtained script-like TiC carbides), the presence of Ti in matrix tends, on the other hand, slowing down Cr diffusion and consequently threatening the chromia-forming behaviour of the alloys. On another side titanium seems having also a beneficial effect on the oxidation behaviour: resistance against spallation during thermal cycling by improving the adherence of the external oxide scale, and maybe on chromia volatilization (re-oxidation of solid $Cr_2O_3$ into gaseous $CrO_3$) by externally covering the chromia scale by a thin outer scale of $TiO_2$ and then isolating chromia from air. These last hypothetic influences of titanium issued from this work need further investigations.

These Ti-containing nickel-based alloys may represent an interesting base for superalloys devoted to the manufacture of pieces geometrically complex to which single crystals cannot be suitable. Pieces made of such alloys can be fabricated using a conventional foundry way (polycrystalline equiaxed microstructures) and exposed in service not only to high temperature stresses and oxidation but also hot corrosion by molten substances (compulsory presence of high amount in chromium instead aluminium). Increase in chromium content from these 25 wt.%Cr to 30 wt.% and more) and reinforcing them again by adding a second MC-former metal more efficient than titanium (Hf for example), may lead to significant improvement in both domains, mechanical and chemical resistance at temperatures as high as 1200°C. This will be subject also to soon further investigations.

*This research did not receive any specific grant from funding agencies in the public, commercial, or not-for-profit sectors.*

## 7. References

[1] Sims, C.H.W. (1972) The superalloys, New York: John Willey

[2] Bradley, E.F. (1988) Superalloys: A Technical Guide, ASM International, Metals Park.

[3] Bradley, E.F. (2002) Superalloys: A Technical Guide (2nd edition), ASM International, Materials Park.

[4] Ikeda, M. Recent trends of research and development of titanium alloy. Denki Seiko, **86(2)**, 45-50 (2015).

[5] Zhai, Y, Lados, D. A., Brown, E. J., Vigilante, G. N. Fatigue crack growth behavior and microstructural mechanisms in Ti-6Al-4V manufactured by laser engineered net shaping. International Journal of Fatigue, **93(1)**, 51-63 (2016).

[6] Wang, C., Dunand, D. C.. Nanoscale cellular structures at phase boundaries of Ni-Cr-Al-Ti and Ni-Cr-Mo-Al-Ti superalloys. Metallurgical and Materials Transactions A: Physical Metallurgy and Materials Science, **46(6)**, 2680-2687 (2015).

[7] Oni, A. A., Broderick, S. R., Rajan, K., LeBeau, J. M. Atom site preference and γ/γ' mismatch strain in Ni-Al-Co-Ti superalloys. Denki Seiko, **86(2)**, 45-50 (2015).

[8] Abbasi, M., Kim, D.-I., Shim, J.-H., Jung, W.-S. Effects of alloyed aluminum and titanium on the oxidation behavior of INCONEL 740 superalloy. Journal of Alloys and Compounds, **658**, 210-221 (2016).

[9] Basuki, E. A., Hajar, D. S., Rahman, F., Prajitno, D. Cyclic oxidation of aluminides coated two phase α2-$Ti_3Al$/γ-TiAl alloys at 1000°C. Procedia Chemistry, **16**, 47-52 (2015).

[10] Chen, B., Xiong, H., Sun, B., Tang, S., Du, B., Li, N. Microstructures and mechanical properties of $Ti_3Al$/Ni-based superalloy joints arc welded with Ti-Nb and Ti-Ni-Nb filler alloys. Progress in Natural Science: Materials International, **24(4)**, 313-320 (2014).

[11] Chen, B., Xiong, H., Sun, B., Tang, S., Guo, S., Zhang, X. Microstructures evolution and tensile properties of $Ti_3Al$/Ni-based superalloy welded joint. Journal of Materials Science and Technology, **30(7)**, 715-721 (2014).

[12] Naffakh-Moosavy, H. Microstructurak investigation and castability anticipation in modern Ti/Al/Nb-containing nickel-based superalloys. Transactions of Non-ferrous Metals Society of China, **26(6)**, 1607-1619 (2016).

[13] Li, F., Fu, R., Yin, F., Feng, D., Wang, H., Du, G., Feng, Y. Impact of γ'($Ni_3$(Al,Ti)) phase on dynamic recrystallization of a Ni-based disk superalloy during isothermal compression. Journal of Alloys and Compounds, **693**, 1076-1082 (2017).

[14] Zhang, P., Ma, L., Yang, G., Song, X. Extraordinary plastic behaviour of the g' precipitate in a directionally solidified nickel-based superalloy. Philosophical Magazine Letters, **96(1)**, 19-26 (2016).

[15] Antonov, S., Detrois, M., Helmink, R. C., Tin, S. Precipitate phase stability and compositional dependence on alloying additions in γ–γ'–δ–n Ni-base superalloys. Journal of Alloys and Compounds, **626**, 76-86 (2015).

[16] Xu, Y., Yang, C., Xiao, X., Cao, X., Jia, G., Shen, Z. Strengthening behavior of Al and Ti elements at room temperature and high temperature in modified Nimonic 80A. Materials Chemistry and Physics, **134(2-3)**, 706-715 (2012).

[17] Kofstad, P. (1988) High Temperature Corrosion, Elsevier Applied Science, London.

[18] Young, D. J. (2008) High temperature oxidation and corrosion of metals, 1st edn; , Elsevier Corrosion Series, Amsterdam.

[19] Benett, R. J., Krakow, R., Eggeman, A. S., Jones, C. N., Murakami, H., Rae, C. M. F. On the oxidation behavior of titanium within coated nickel-based superalloys. Acta Materialia, **92**, 278-289 (2015).

[20] Weng, F., Yu, H., Chen, C., Wan, K. High-temperature oxidation behavior of Ni-based superalloys with Nb and Y and the interface characteristics of oxidation scales. Surface and Interface Analysis, **47(3)**, 362-370 (2015).

[21] Khair, M., Berthod, P. As-cast microstructures and hardness of chromium-rich cobalt-based alloys reinforced by titanium carbides. Materials Science: An Indian Journal, **14(13)**, in press.

[22] Berthod, P., Conrath, E. Microstructure evolution in bulk and surface states of chromium rich nickel based cast alloys reinforced by hafnium carbides after exposure to high temperature air. Materials at High Temperature, **31(3)**, 266-273 (2014).

[23] Shatynski, S. R. The thermochemistry of transition metal carbides. Oxidation of Metals, **13(2)**, 105-118 (1979).

[24] Berthod, P., Allègre, F., Kretz, E., Khair, M., Ritouet, M. High temperature properties of several families of TiC-reinforced cast superalloys, “Beyond Nickel-Based Superalloys II”, July 17-21, 2016 (Cambridge, United Kingdom).

[25] Berthod, P. Nouveaux superalliages de fonderie equiaxe base nickel et base cobalt renforcés par carbures HfC pour utilization à 1100°C et plus. Journées annuelles SF2M « Matériaux pour le domaine aérospatial : de l’innovation dans l’air », Octobert 25-27, 2016 (Albi, France).

[26] Ritouet, M., Berthod, P. Behavior in high temperature oxidation of a cast nickel-based superalloy reinforced by niobium carbides. “High Temperature Corrosion and Protection of Materials HTCPM9”, May 15-20, 2016 (Les Embiez, France).

[27] Berthod, P., Aranda, L., Vébert, C., Michon, S. Experimental and Thermodynamic Study of the Microstructural State at High Temperature of Nickel base Alloys containing Tantalum. Calphad, **28(2)**, 159-166 (2004).

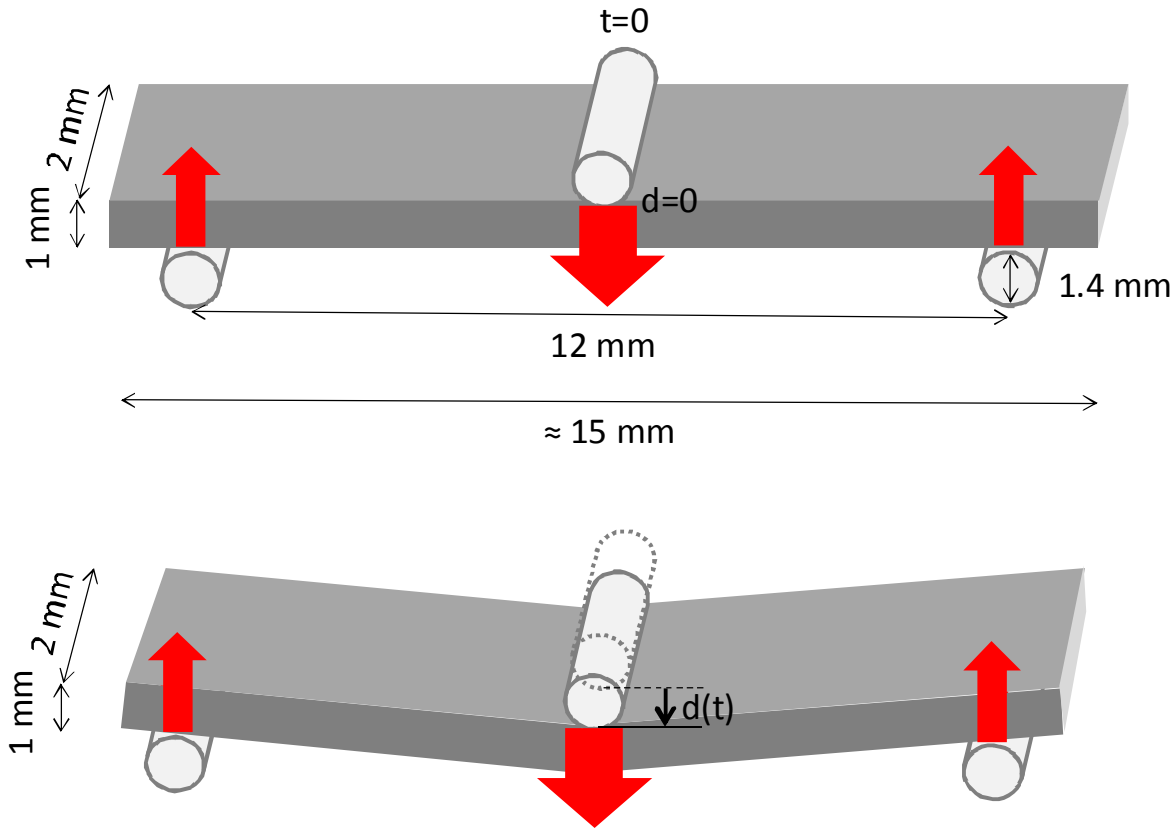


Fig. 1. Scheme explaining the principle of the 3-points flexural creep test (top: initial position, bottom: progressive displacement of the upper central point due to creep, plotted to obtain the creep deformation curve)

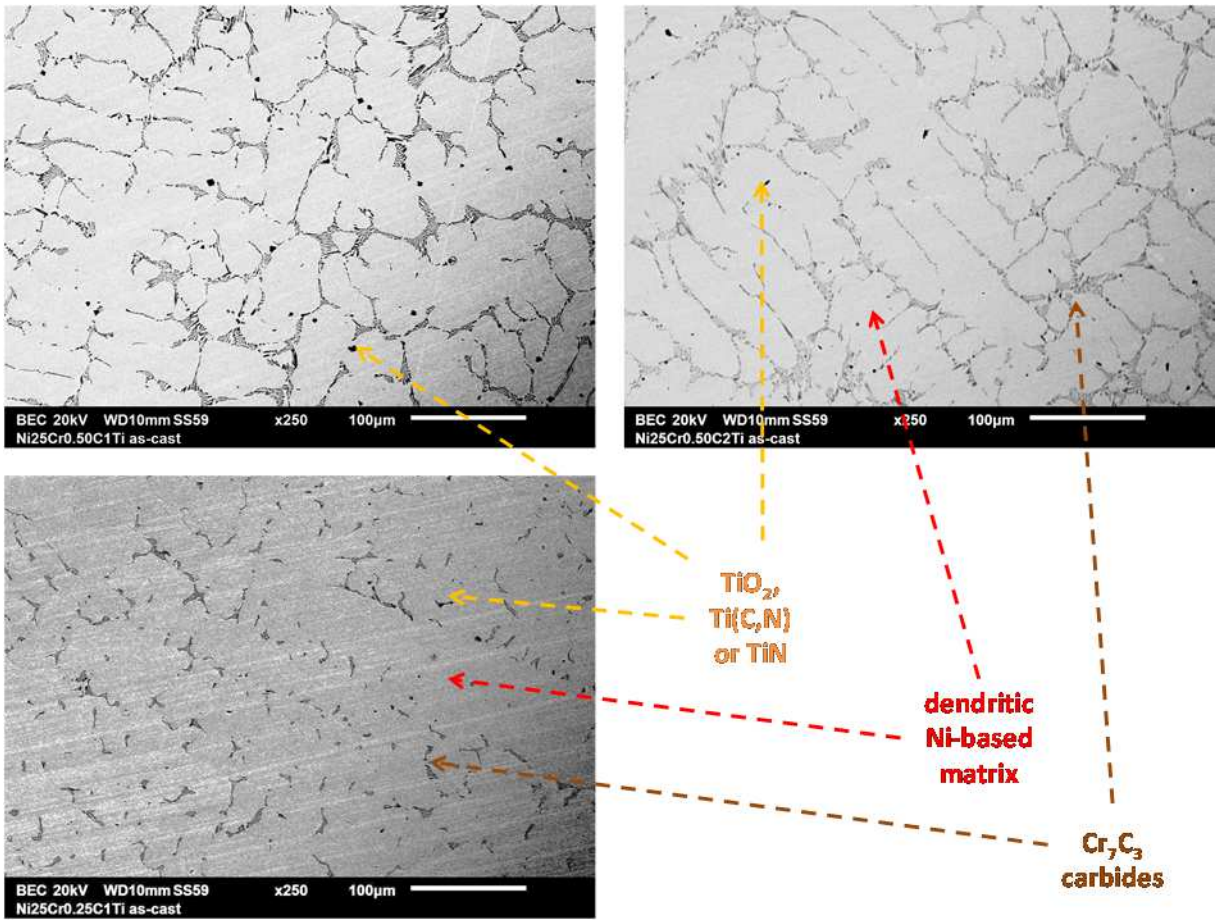


Fig. 2. Large view of the microstructures of the three alloys in their as-cast state (SEM/BSE micrographs)

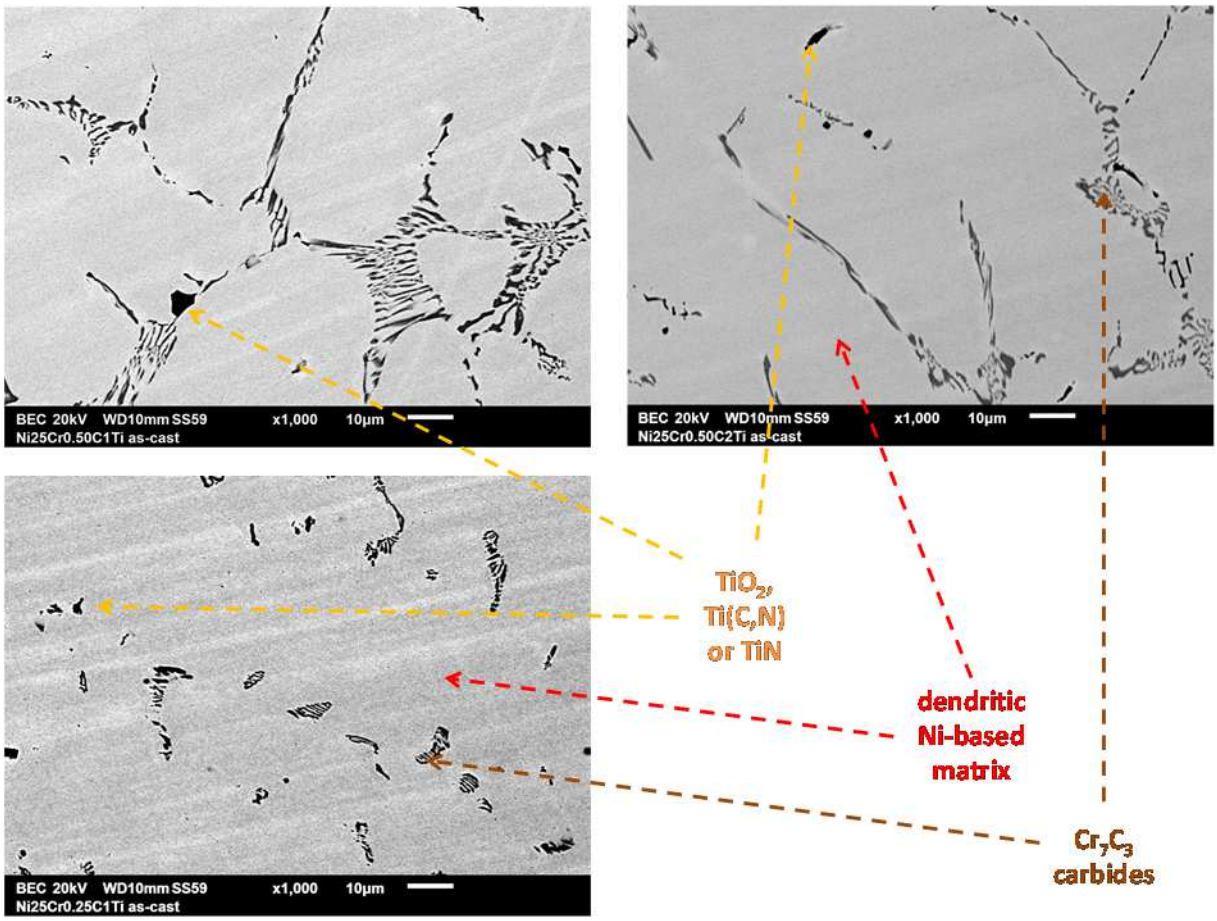


Fig. 3. Detailed view of the microstructures of the three alloys in their as-cast state (SEM/BSE micrographs)

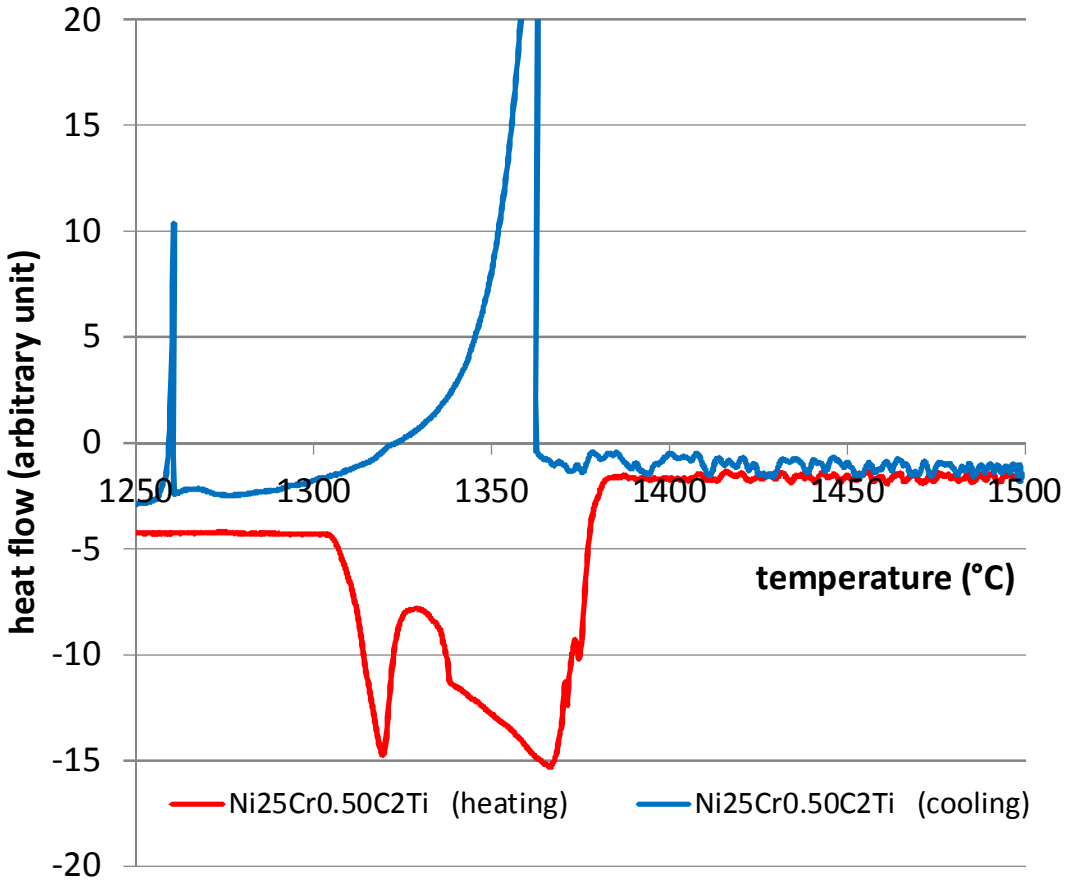


Fig. 4. One of the DTA curves obtained (here: the Ni-25Cr-0.50C-2Ti alloy)

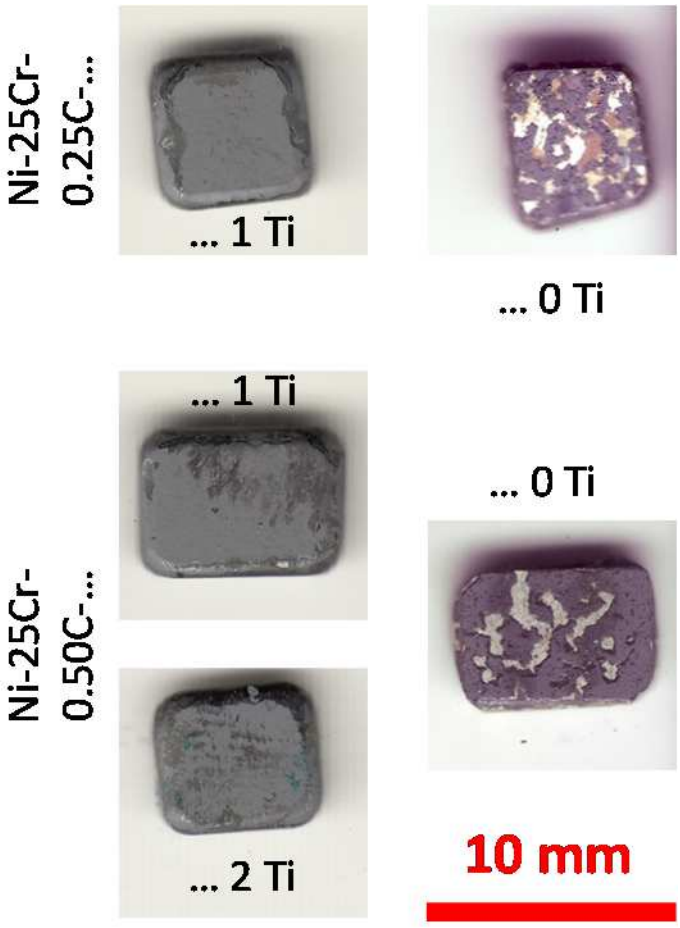


Fig. 5. Illustration of the better resistance against oxide spallation at cooling demonstrated by the three studied Ti-containing alloys (left) than the corresponding Ti-free alloys for the same operating parameters (earlier study)

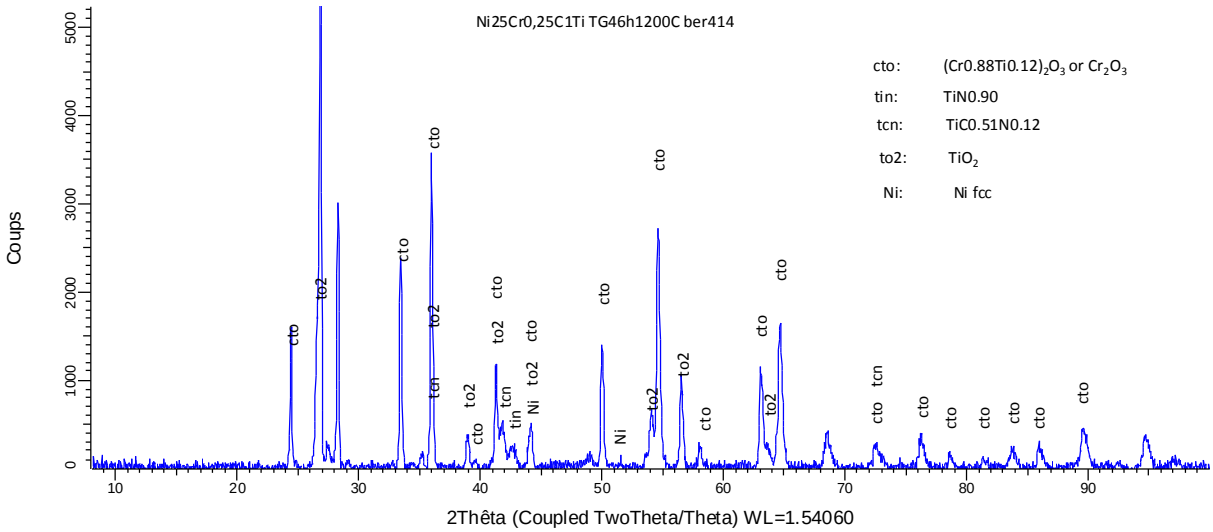


Fig. 6. Example of diffractogram acquired on the oxidized surfaces of the aged Ti-containing alloys (here: Ni-25Cr-0.50C-1Ti)

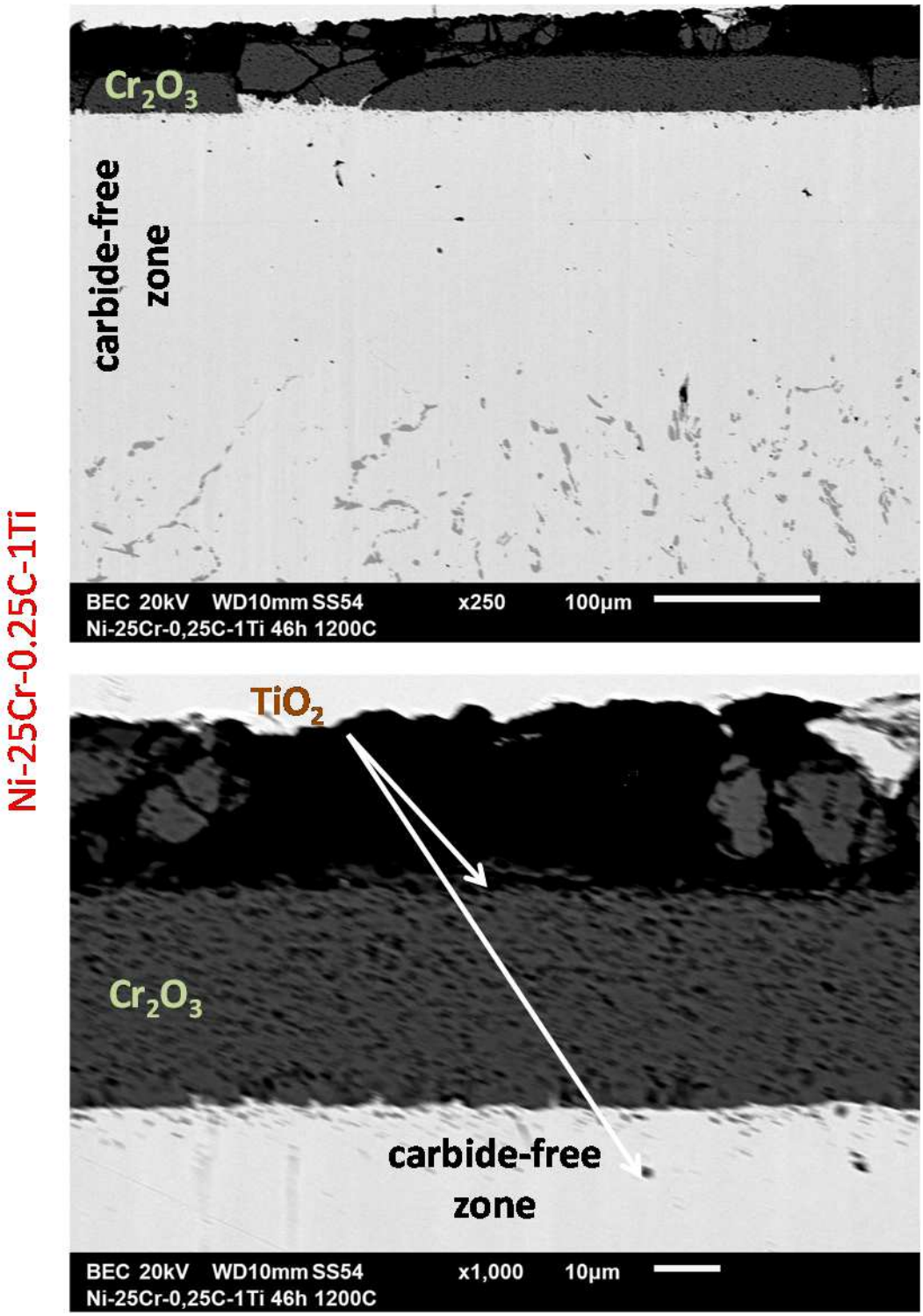


Fig. 7. General (top) and detailed (bottom) views of the surface state of the aged Ni-25Cr-0.25C-1Ti alloy (SEM/BSE micrographs)

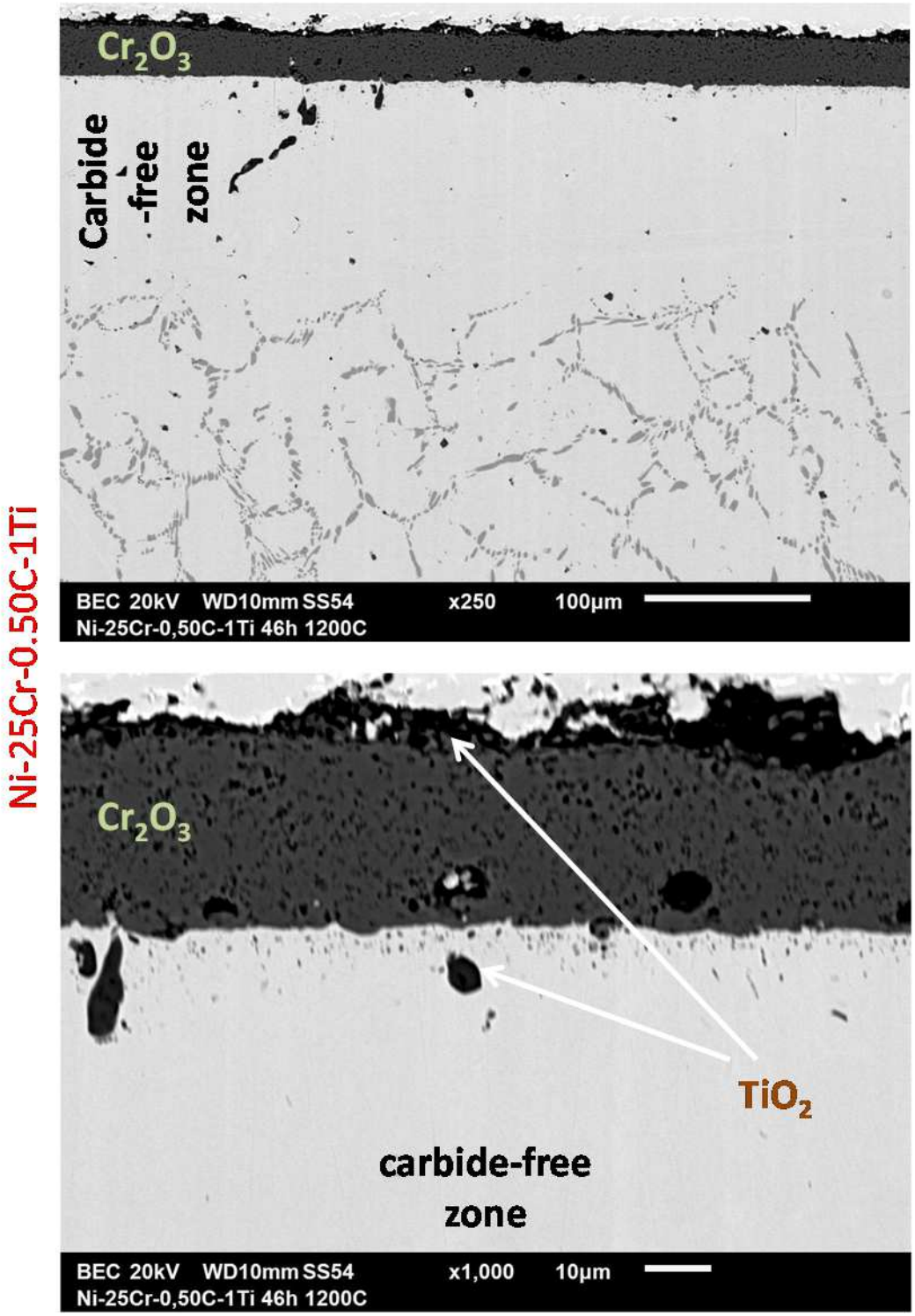


Fig. 8. General (top) and detailed (bottom) views of the surface state of the aged Ni-25Cr-0.50C-1Ti alloy (SEM/BSE micrographs)

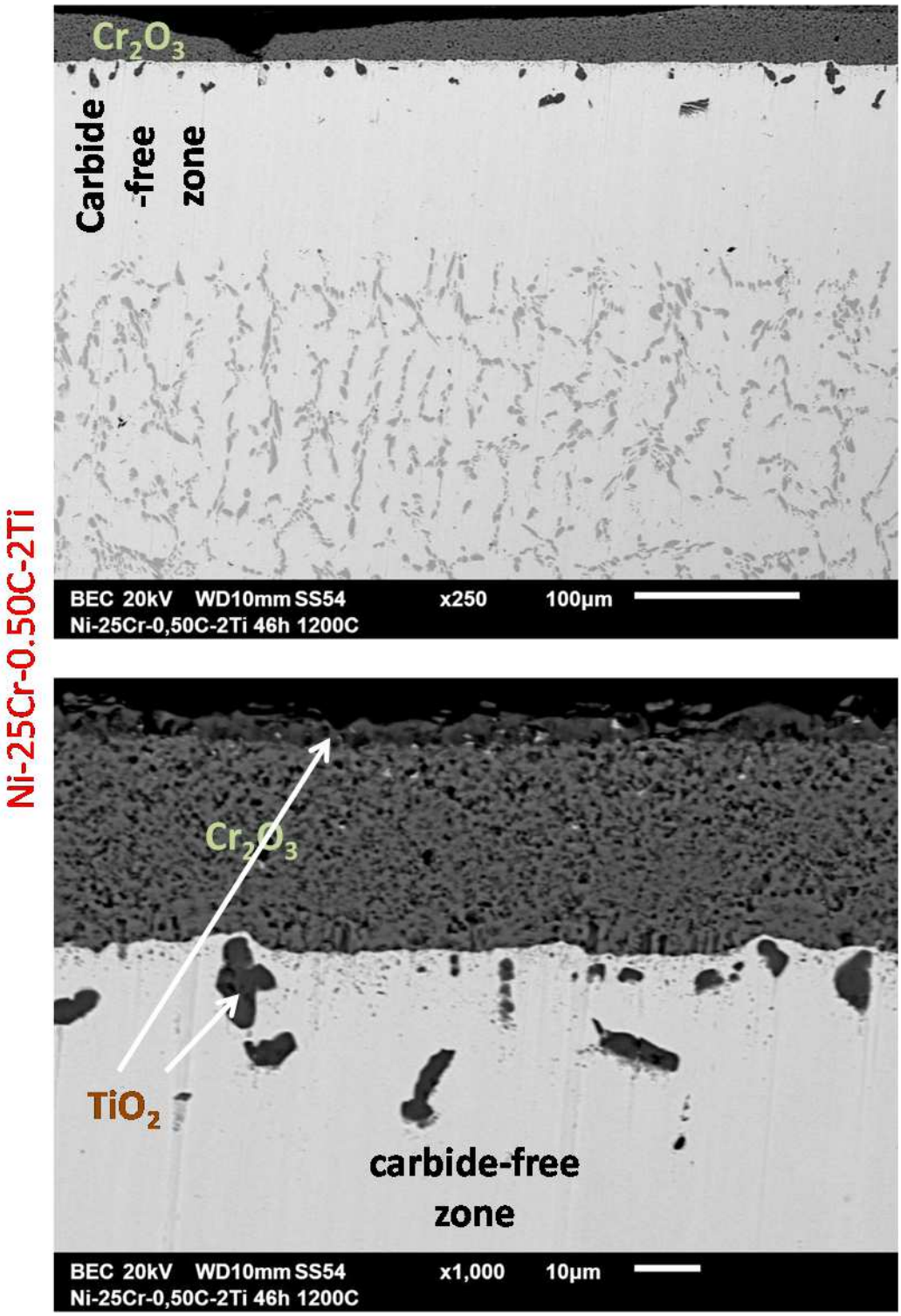


Fig. 9. General (top) and detailed (bottom) views of the surface state of the aged Ni-25Cr-0.50C-2Ti alloy (SEM/BSE micrographs)

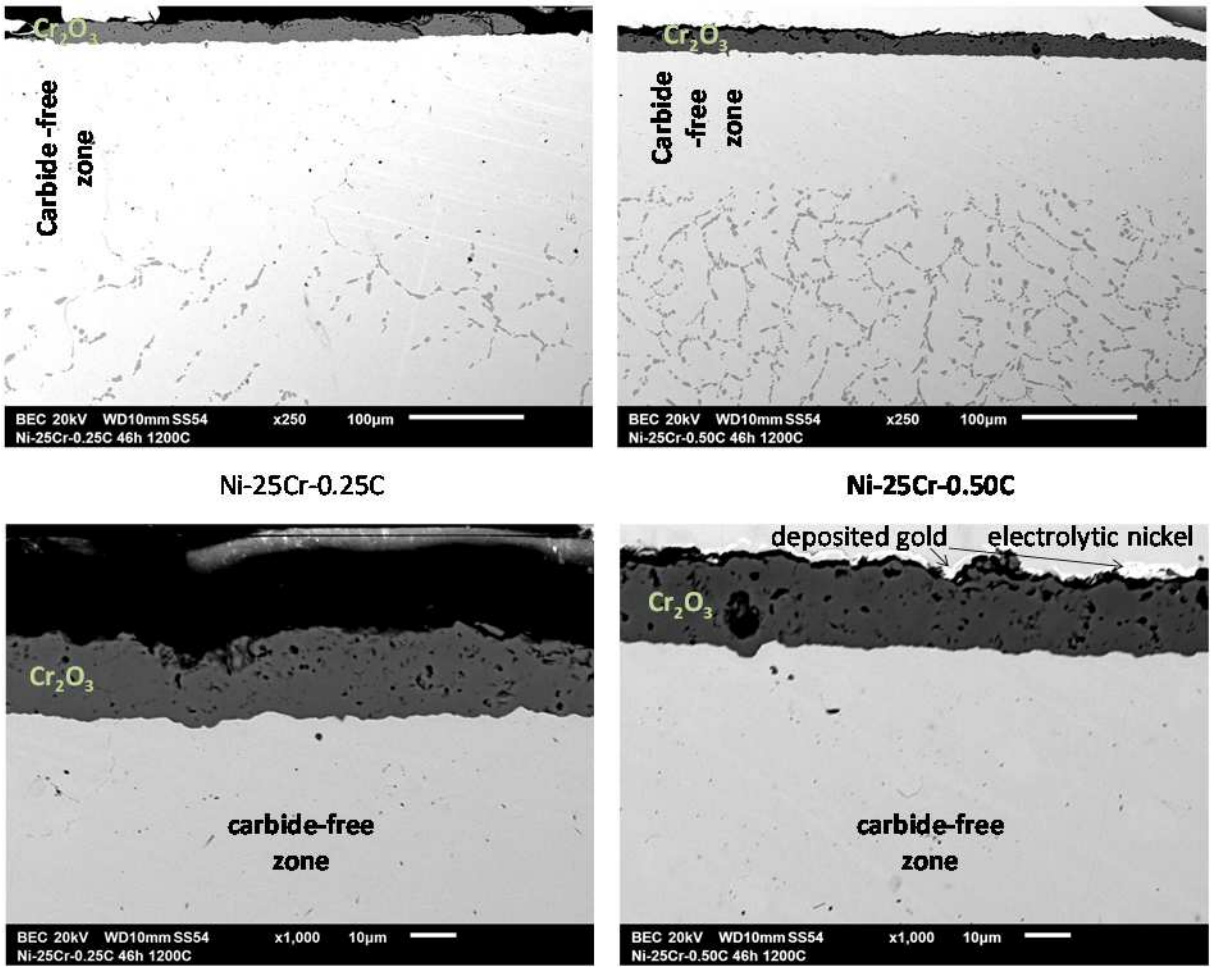


Fig. 10. General (top) and detailed (bottom) views of the surface state of aged Ti-free ternary Ni-25Cr-0.25C and Ni-25Cr-0.50C alloys for comparison (SEM/BSE micrographs)

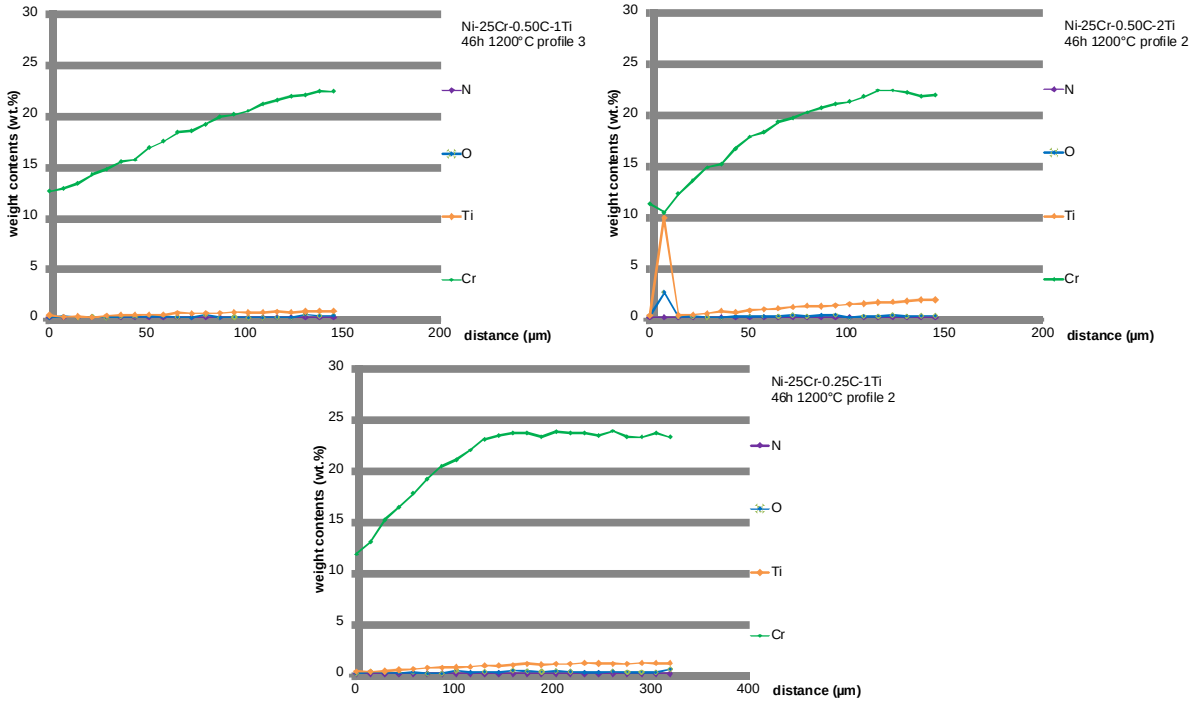


Fig. 11. Concentration profiles acquired perpendicularly to the oxide scale/alloy interface, from this interface to the first bulk not affected by oxidation; here the three Ti-containing alloys: Ni-25Cr-0.25C-1Ti (bottom), Ni-25Cr-0.50C-1Ti (top left), and Ni-25Cr-0.50C-2Ti (top right)

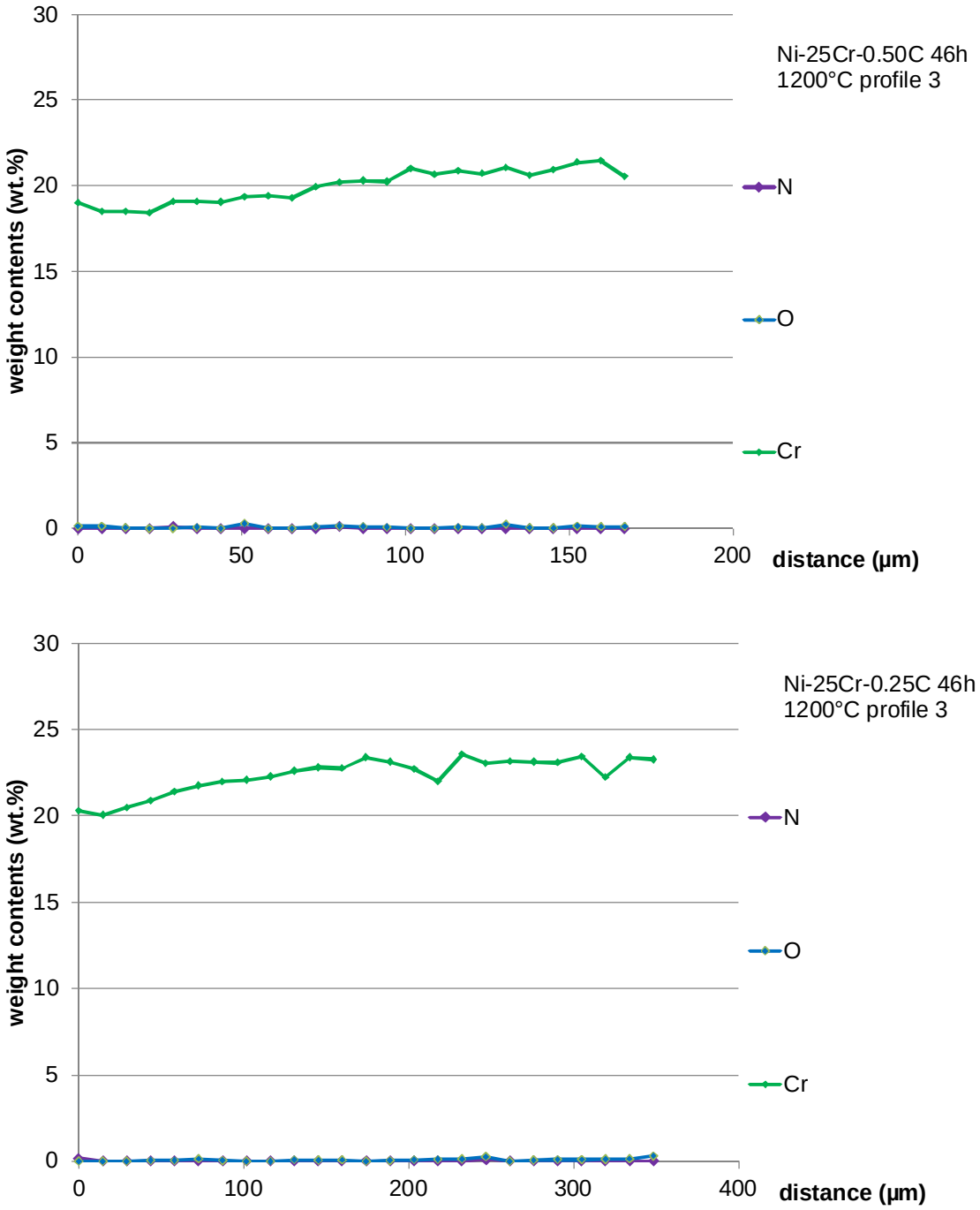


Fig. 12. Concentration profiles acquired perpendicularly to the oxide scale/alloy interface, from this interface to the first bulk not affected by oxidation, here for the two ternary reference alloys: Ni-25Cr-0.25C (bottom) and Ni-25Cr-0.50C (top)

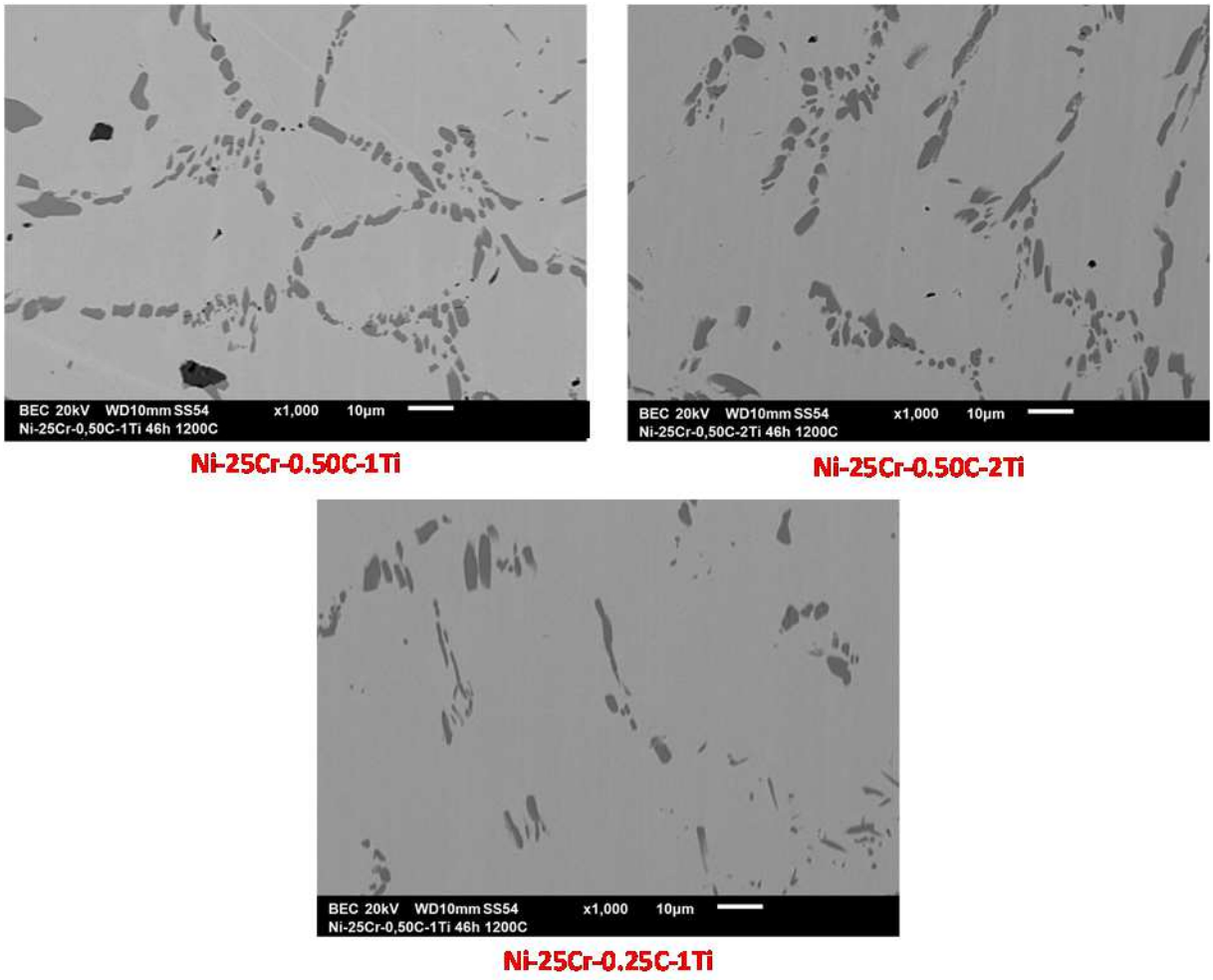


Fig. 13. Bulk microstructure states of the three Ti-containing alloys after 46 hours spent at 1200°C: Ni-25Cr-0.25C-1Ti (bottom), Ni-25Cr-0.50C-1Ti (top left), and Ni-25Cr-0.50C-2Ti (top right)

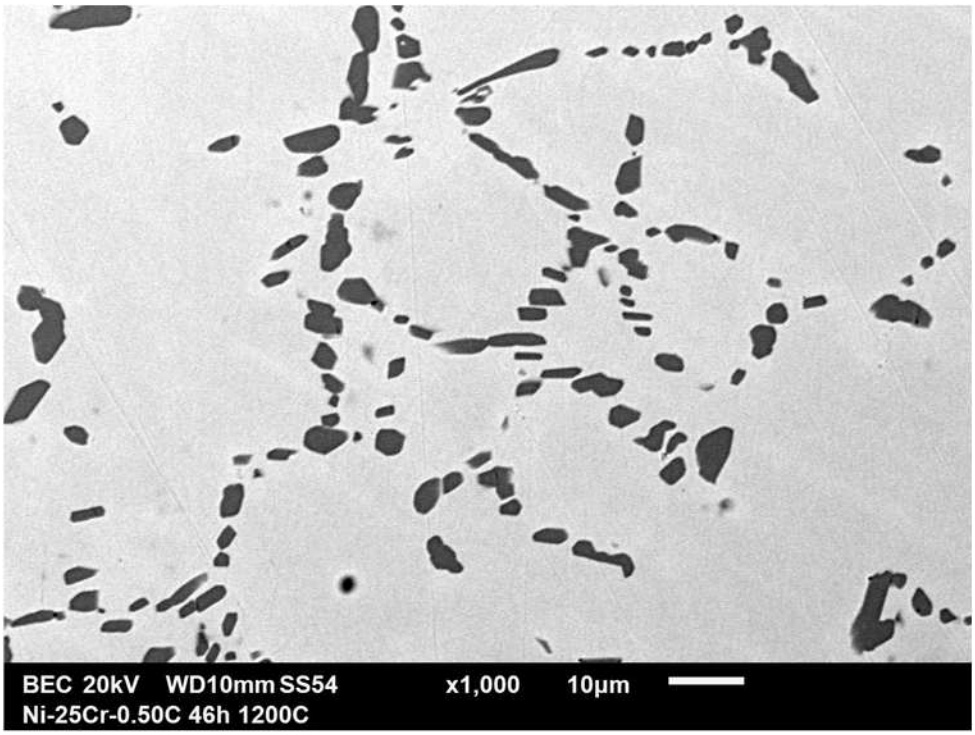


Fig. 14. Bulk microstructure states of the two reference Ti-free alloys after 46 hours spent at 1200°C: Ni-25Cr-0.25C (bottom) and Ni-25Cr-0.50C (top)

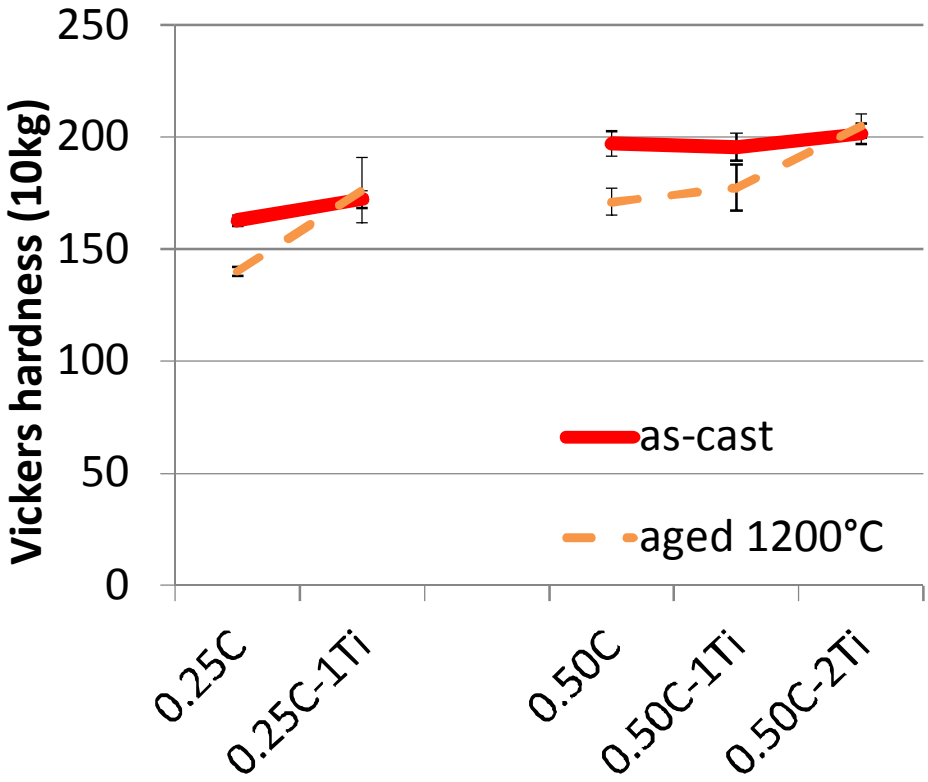


Fig. 15. The hardness values of the Ti-containing alloys in their as-cast states and their {46h, 1200°C}-aged states; comparison with the ternary alloys

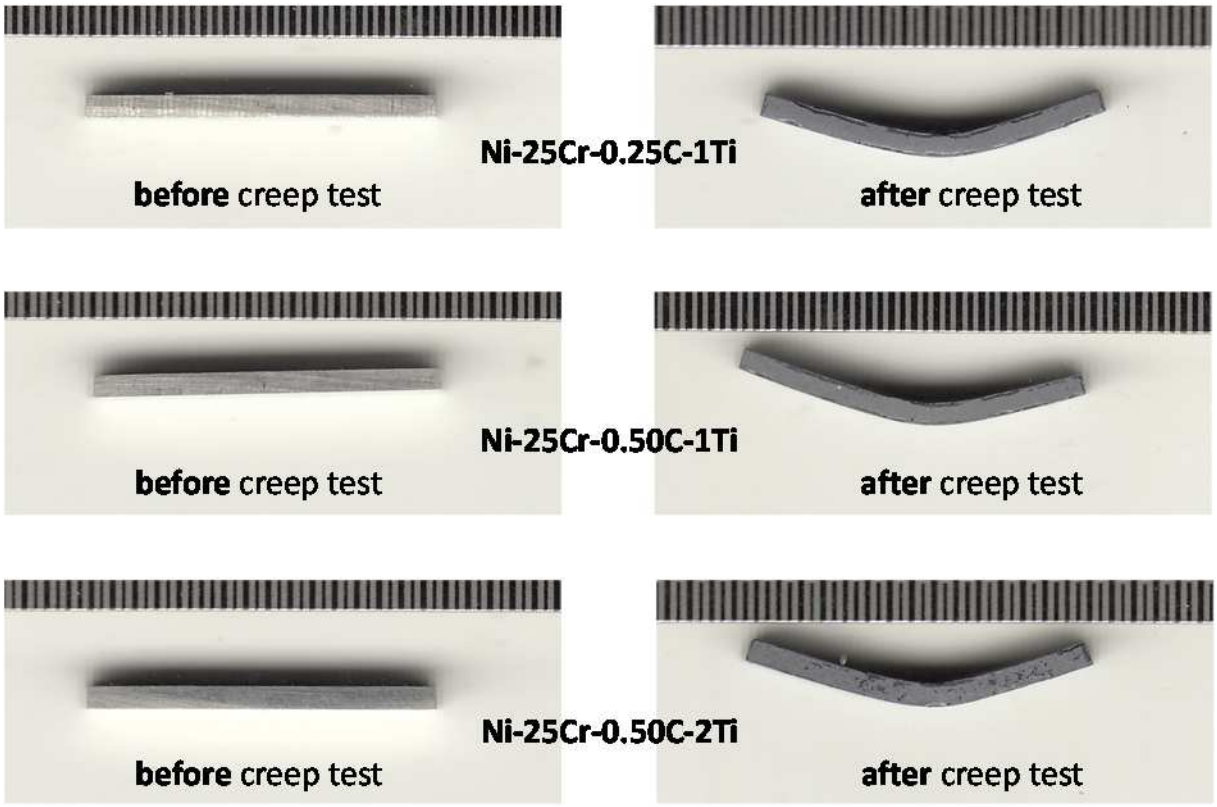


Fig. 16. Photographs of the creep samples before and after the {20MP, 1200°C}-creep tests

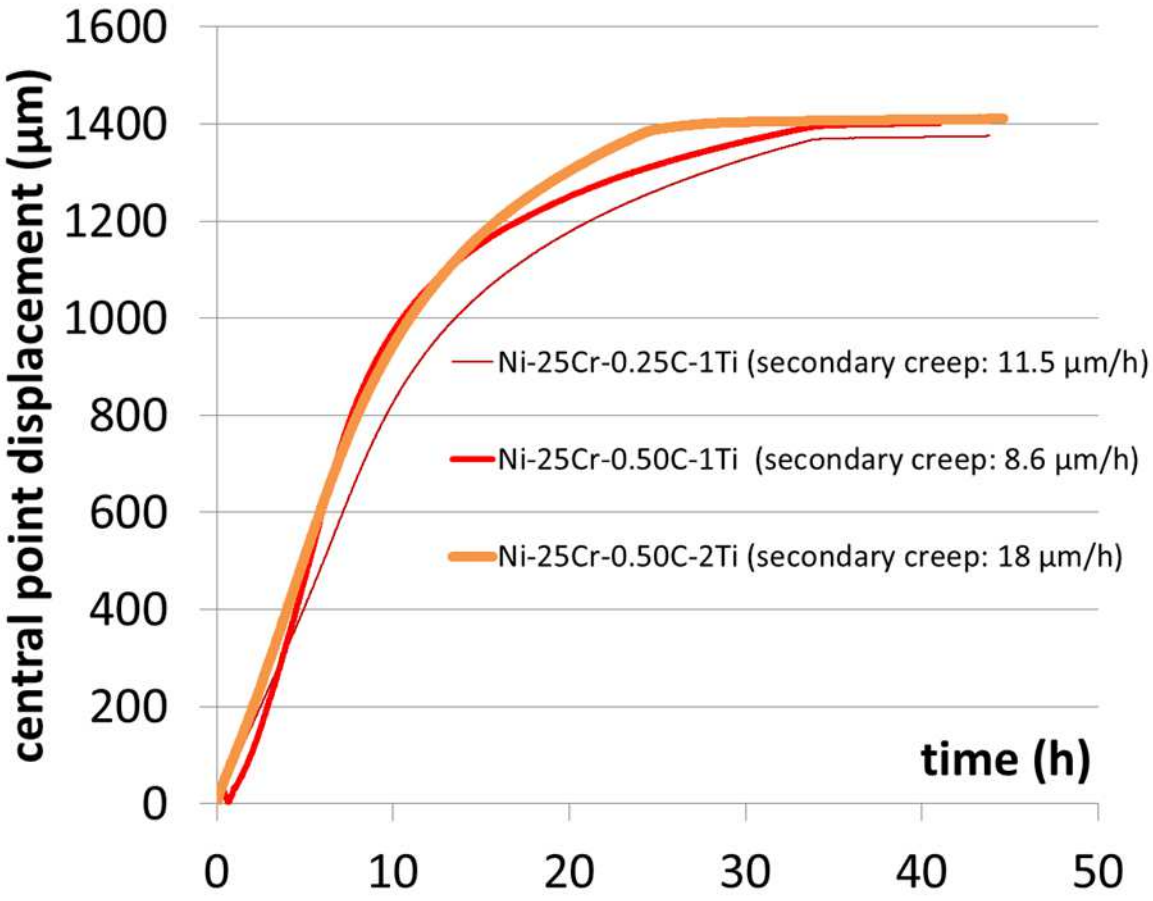


Fig. 17. The obtained {20MP, 1200°C}-creep deformation curves

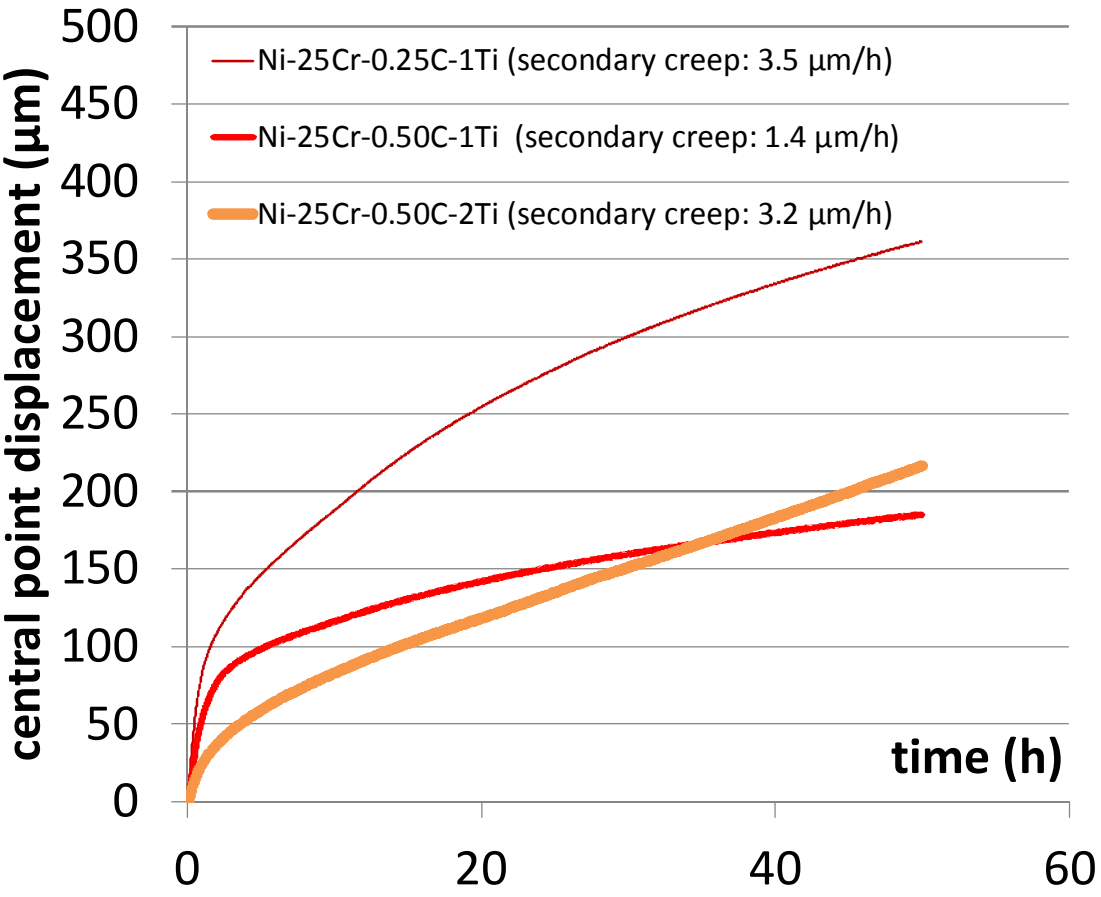


Fig. 18. The obtained {5MP, 1200°C}-creep deformation curves

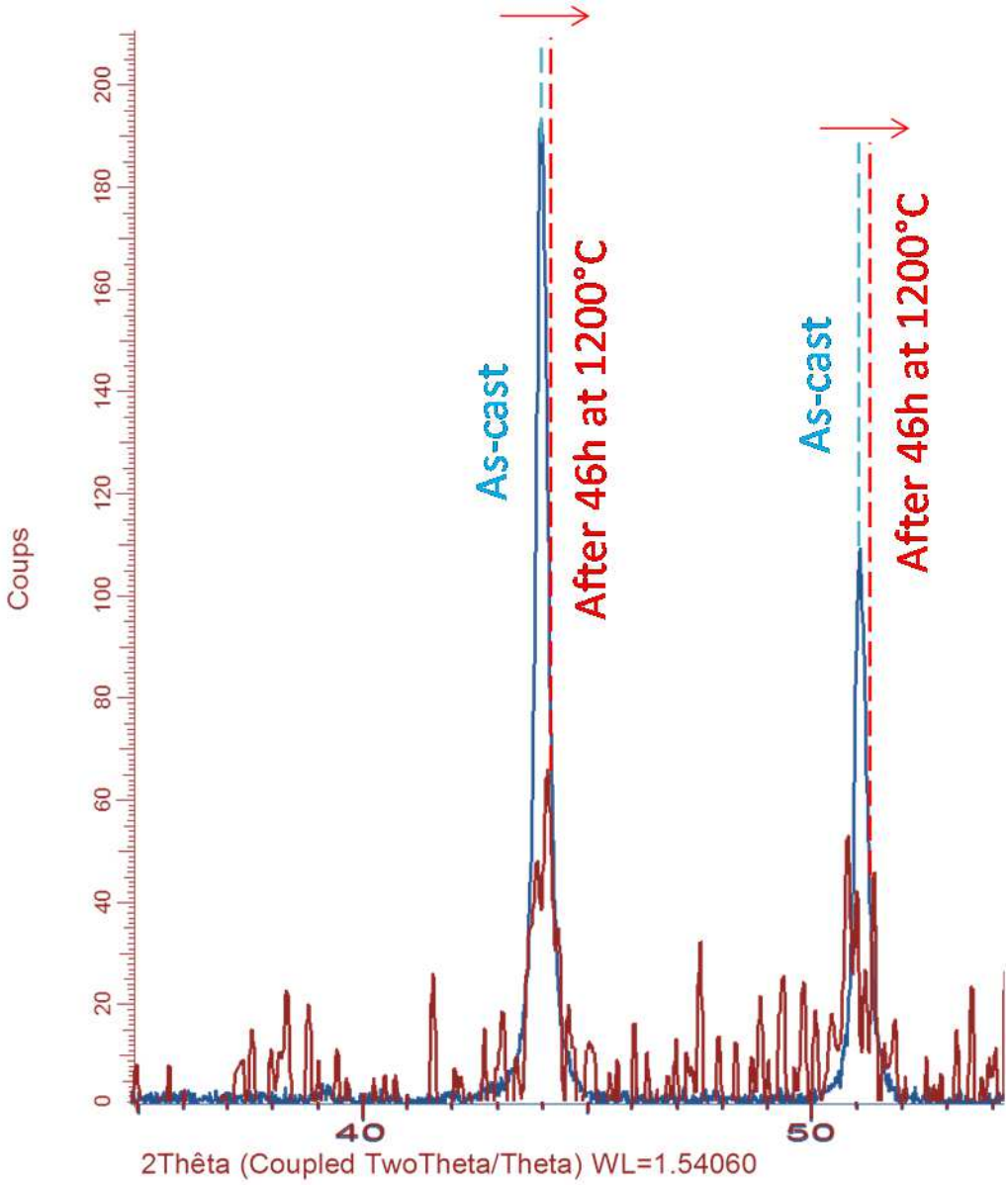


Fig. 19. Peaks' shift toward higher angles by the presence of more Ti atoms in the austenitic network of the Ni(Cr) matrix due to the disappearance, during the exposure at 1200°C, of the rare TiC carbides initially present in the as-cast Ni-25Cr-0.50C-2Ti alloy (spectrum locally enlarged to allow visualizing the slight shift)